Neurodegeneration and defective neurotransmission in a *Caenorhabditis elegans* model of tauopathy

Brian C. Kraemer*†, Bin Zhang‡, James B. Leverenz§¶‖, James H. Thomas, John Q. Trojanowski‡, and Gerard D. Schellenberg*†,††‡‡§§**

*Geriatrics Research Education and Clinical Center and ‖Mental Illness and Parkinson Disease Research Education and Clinical Center, Veterans Affairs Puget Sound Health Care System, Seattle, WA 98108-1597; Departments of §Neurology, ¶Psychiatry and Behavioral Sciences, **Genome Sciences, and ‡‡Pharmacology, †Division of Gerontology and Geriatric Medicine, Department of Medicine, and ††Division of Neurogenetics, Department of Neurology, University of Washington, Seattle, WA 98195; and ‡Center for Neurodegenerative Disease Research, Department of Pathology and Laboratory Medicine, University of Pennsylvania School of Medicine, Philadelphia, PA 19104

Communicated by Ralph M. Garruto, Binghamton University, Binghamton, NY, June 9, 2003 (received for review April 15, 2003)

Frontotemporal dementia with parkinsonism chromosome 17 type (FTDP-17) is caused by mutations in *MAPT*, the gene encoding tau. FTDP-17 begins with executive function deficits and other abnormal behaviors, which progress to dementia. Neurodegenerative changes include accumulation of aggregated tau as neuronal and glial fibrillary tangles. Aggregated tau is seen in numerous other neurodegenerative diseases, including Alzheimer's disease (AD). We expressed normal and FTDP-17 mutant human tau (mutations $^{P}301^{L}$ and $^{V}337^{M}$) in *Caenorhabditis elegans* to model tauopathy disorders. Tau pan-neuronal expression caused progressive uncoordinated locomotion (Unc), characteristic of nervous system defects in worms. Subsequently, insoluble tau accumulates and both soluble and insoluble tau is phosphorylated at many of the sites hyperphosphorylated in FTDP-17, AD, and other tauopathies. Substantial neurodegeneration, seen as bulges and gaps in nerve cords followed by loss of neurons, occurs after insoluble tau begins to accumulate. Axons show vacuoles, membranous infoldings, and whorls with associated amorphous tau accumulations and abnormal tau-positive aggregates. FTDP-17 mutation lines had a more severe Unc phenotype, accumulated more insoluble tau at a younger age, were more resistant to cholinergic inhibitors, and had more severe axonal degeneration when compared with lines expressing normal tau. The Unc phenotype is caused by a presynaptic defect. Postsynaptic transmission is intact. This transgenic model will enable mechanistic dissection of tau-induced neurodegeneration and identification of genes and compounds that inhibit pathological tau formation.

Abnormally aggregated tau accumulates as neurofibrillary tangles and other lesions in many neurodegenerative diseases including Alzheimer's disease (AD) and frontotemporal dementia with parkinsonism chromosome 17 type (FTDP-17). For AD and most tauopathies, the role tau plays in disease initiation and progression is unknown. However, in FTDP-17, mutations in *MAPT*, the gene encoding tau, cause the disease (1–3), albeit by incompletely understood mechanisms. One hypothesis is that microtubule (MT)-mediated axonal transport is disrupted, an idea based on the reduced binding affinity of mutant tau for MTs (4). Another hypothesis is that aggregated tau is deleterious to cells, and in FTDP-17, aggregation is driven by either increased free tau concentrations (4) or mutation-induced acceleration of self-aggregation (5, 6). The critical toxic aggregate may be a dimer, a more extensive aggregate, tau filaments, or the end-stage tangles. The phosphorylation state of tau may also be important, as pathologic insoluble tau is hyperphosphorylated (7).

To identify critical steps in tau-induced neurodegeneration, we generated a *MAPT* transgenic (Tg) *Caenorhabditis elegans* model of FTDP-17. Pan-neuronal expression of normal or FTDP-17 mutant *MAPT* resulted in altered behavior (uncoordinated movement), accumulation of insoluble phosphorylated tau, age-dependent loss of axons and neurons, and structural damage of axonal tracks. This degenerative phenotype was more severe in Tg lines expressing FTDP-17 mutant tau compared with lines expressing normal tau. Tau expression caused defective presynaptic cholinergic transmission. Abnormal behavior occurred before accumulation of insoluble tau and neuronal loss, suggesting that aggregation is not required for tau-induced neuronal dysfunction.

Methods

Strains. Bristol strain N2 was the wild-type *C. elegans*. For aldicarb and levamisole experiments, strains *unc-29*(e1072), *unc-31*(e928), and *unc-64*(e246) were used. Strain CZ1200 carries an integrated *unc*-25::gfp transgene. Strain *glp-4*(bn2) is fertile when grown at 15°C and sterile when grown at 25°C.

Tg Lines. Human 4R1N tau and the *aex-3* promoter (8) were inserted into vector pPD49.26. FTDP-17 mutations $^{V}337^{M}$ and $^{P}301^{L}$ were introduced by site-directed mutagenesis. Strain N2 was injected with *aex*-3::tau constructs and *myo-2*::GFP to produce worms with tau and GFP transgenes as extrachromosomal arrays. Transgenes were integrated by exposing animals to x-rays, and animals were out-crossed five times.

Behavioral Assays. Liquid thrashing assays were performed in 20 μl of M9 media (42 mM Na_2HPO_4/22 mM KH_2PO_4/86 mM NaCl/1 mM $MgSO_4$) on a Teflon-printed slide. Worms were allowed to settle, and thrashes were counted for 30 sec. Lifespans were measured as described (9). Animals that died by internal embryo hatching were not counted.

Protein Extraction. Tau fractions were obtained (10) by resuspending pelleted worms in an equal amount (wt/vol) of high salt RAB buffer (100 mM Mes/1 mM EGTA/0.5 mM $MgSO_4$/20 mM NaF). Worms were lysed by sonication, and homogenates were centrifuged at 40,000 $\times$ *g* for 40 min. The supernatant constitutes the RAB fraction. The pellet was reextracted with 1 M sucrose in RAB buffer and centrifuged 20 min at 40,000 $\times$ *g*, and the supernatant was discarded. The pellet was extracted with RIPA buffer (150 mM NaCl/1% Nonidet P-40/0.5% deoxycholate/0.1% SDS/50 mM Tris, pH 8.0) and centrifuged at 40,000 $\times$ *g* for 20 min. The supernatant is the RIPA fraction. The pellet was extracted with 70% formic acid (FA) and centrifuged at 13,000 $\times$ *g* for 15 min. The supernatant is the FA fraction. All buffers contained Complete Protease Inhibitor mixture (Roche Diagnostics) and 0.5 mM PMSF.

Immunoblotting. For quantitative immunoblotting, human tau was detected with antibody T46 or 17026. *C. elegans* β-tubulin

Abbreviations: AD, Alzheimer's disease; FTDP-17, frontotemporal dementia with parkinsonism chromosome 17 type; MT, microtubule; Unc, uncoordinated locomotion; Tg, transgenic; FA, formic acid; EM, electron microscopy.

See commentary on page 9653.

§§To whom correspondence should be addressed. E-mail: zachdad@u.washington.edu.

www.pnas.org/cgi/doi/10.1073/pnas.1533448100

levels were measured by using antibody E7 as an internal control. ^{125}I-labled goat anti-mouse IgG was the secondary antibody (New England Nuclear), and signals were quantitated by using a Packard Cyclone phosphorimager. Dilutions were 1:3,000 for T46 and 17026; 1:250 for PHF-1 and CP13; 1:1,000 for Tau-2 (Sigma) and 12E8; 1:200 for AT8; 1:500 for pS422 (BioSource International, Camarillo, CA); and 1:15,000 for AT270 (Innogenetics, Ghent, Belgium).

Pharmacological Assays. Aldicarb and levamisole resistance were determined by placing 20 young adult animals on freshly seeded NGM plates containing 1 mM aldicarb (ChemService, West Chester, PA) or 100 μM levamisole (Sigma). After 8 and 2 h, respectively, worms were scored as motile if they exhibited locomotion or pharyngeal pumping when prodded.

Immunohistochemistry. *C. elegans* specimens were fixed overnight in 10% formalin at 4°C, preembedded in Histogel (Richard-Allan Scientific, Kalamazoo, MI), and processed for paraffin embedding. Blocks were cut into 10-μm sections and immunostained (11). Antibody dilutions were 1:250 for Tau-2, 1:500 for T46, and 1:100 for PHF-1 and CP13.

Transmission Electron Microscopy (EM). Worms were anesthetized with 8% ethanol, then immersed in 10 ml of 2% glutaraldehyde and 2% paraformaldehyde in 0.1 M cacodylate buffer. The worms were cut into two segments and kept at 4°C overnight on a shaker. Samples were postfixed in 1% osmium tetroxide in 0.1 M phosphate buffer (pH 7.4) for 1 h at 4°C, rinsed with M9 buffer three times for a total 30 min, stained with 2% uranyl acetate for 1 h at 4°C, and then rinsed again with M9 buffer three times for 30 min. The fixed worm segments were embedded in 1% agarose, sectioned, stained, and examined by using a JEM1010 EM (JEOL) at 80 kV (12).

Preembedding Immuno-EM. Worms were anesthetized with 8% ethanol, immersed in 10 ml of 0.2% glutaraldehyde, 4% paraformaldehyde and 0.2% picric acid in 0.1 M cacodylate buffer, pH 7.3, cut into segments, and shaken in fixative 2 h at 4°C. Worms were embedded in 6% agarose and cut into 50-μm-thick sections with a vibratome, and sections were quenched in 0.1% sodium borohydride in Tris-buffered saline for 10 min and 20% ethanol for 10 min. Sections were blocked in 5% horse serum in PBS with 0.1% cold aqueous fish skin gelatin and 1% chicken egg albumin for 60 min, incubated with antibody 17026 (1:1,000 dilution) in 0.1% BSA and PBS and shaken overnight at 4°C. Subsequently, sections were washed and incubated with biotinylated goat anti-rabbit IgG for 2 h at room temperature. Tau-positive profiles in the sections were visualized with diaminobenzidine followed by silver–gold intensification after incubation with silver methenamine developer containing 3% methenamine, 5% silver nitrate and 1% sodium tetraborate at 60°C for 10 min as described (13, 14). The reaction was stopped with 2% sodium acetate and then stabilized in 3% sodium thiosulphate for 5 min. Gold toning was obtained by incubating the sections in 0.1% gold chloride for 5 min, followed by stabilizing with 3% sodium thiosulfate for 5 min. Sections were fixed with 2% glutaraldehyde in PBS buffer overnight. Sections with positive staining were postfixed in 0.5% osmium tetroxide for 20 min at 4°C, dehydrated with graded ethanol solutions, and embedded in Epon-Araldite resin at 60°C for 48 h. Ultrathin sections of these blocks were cut and mounted on 100 mesh EM grids, and examined by using a JEM1010 EM at 80 kV (12).

Results

Tau-Induced Behavioral Defects. We generated *C. elegans* lines that express human 4R1N tau in all neurons. The 4R1N isoform has four MT binding repeats (4R) and one amino terminal (1N) insert and is the most abundant adult human brain isoform. Chromosomally integrated Tg lines were generated by using normal tau (N-1 and N-2), and tau with FTDP-17 mutations $^{V}337^{M}$ (337^{M}-1 and 337^{M}-2) and $^{P}301^{L}$ (301^{L}-1 and 301^{L}-2) (1, 2). *In vitro*, these mutations reduce tau binding affinities to MTs (4), and accelerate tau aggregation (15, 16). All lines also express GFP in the pharynx.

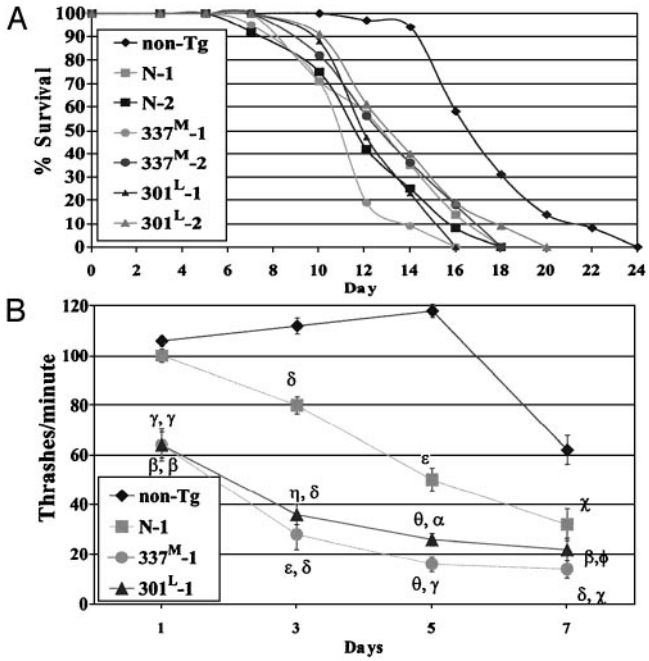

Fig. 1. (*A*) Tg worm lifespans. Average lifespans in days (±SD) are: N-1, 11.1 ± 0.8; N-2, 12.6 ± 0.8; 337^{M}-1, 10.9 ± 0.4; 337^{M}-2, 12.8 ± 0.3; 301^{P}-1, 12.3 ± 0.3; and 301^{P}-2, 13.31 ± 0.5. Lifespans for each Tg line was different from the non-Tg line ($P < 10^{-4}$ to $P < 10^{-12}$; two-tailed *t* test) but not different from other Tg lines. (*B*) Unc phenotype and age. Each point is the mean thrashing rate for 10 developmentally staged non-Tg, N-1, 337^{M}-1, or 301^{L}-1 animals. Error bars are the SEM. For N-1, symbols are for comparison to non-Tg values. For 301^{L} and 337^{M}-1, the first symbol is for comparisons to non-Tg and the second symbol is for comparisons to N-1. Symbols are as follows: Φ, $P < 0.2$; χ, $P < 1 \times 10^{-2}$; α, $P < 1 \times 10^{-3}$; β, $P < 1 \times 10^{-4}$; γ, $P < 1 \times 10^{-5}$; δ, $P < 1 \times 10^{-6}$; ε, $P < 1 \times 10^{-9}$; η, $P < 1 \times 10^{-10}$; θ, $P < 1 \times 10^{-15}$.

Tau expression caused decreased lifespan, uncoordinated locomotion (Unc) (Fig. 1), reduced egg laying (Egl-d), and dumpiness (Dpy), phenotypes observed in other *C. elegans* neuronal defect mutants (17–19). The Dpy and Egl-d phenotypes were incompletely penetrant. Unc behavior was frequently visible after hatching. Maturing animals became progressively more Unc, showing partial paralysis, slowed movement, coiling, and intermittent tail dragging, becoming nearly immobile by age 9 days. In liquid, *C. elegans* thrash rapidly, and Unc animals thrash less. When compared with non-Tg worms, all Tg lines showed reduced thrash rates that declined with age (Fig. 1*B* and Fig. 7, which is published as supporting information on the PNAS web site, www.pnas.org). 301^{L} and 337^{M} lines had lower thrash rates than normal tau lines, with the 337^{M} lines being the most severely affected. The difference in phenotype severity between mutant and normal lines is not caused by differences in tau levels. In all six lines, tau expression levels were comparable with somewhat higher expression in N-1 and N-2 compared with mutant tau lines (Fig. 7*A*). For extrachromosomal array Tg worms, the amount of transgene injected directly correlated with the Unc phenotype severity (Fig. 7*B*). Thus, the fact that the mutant lines had a more severe phenotype than the normal tau

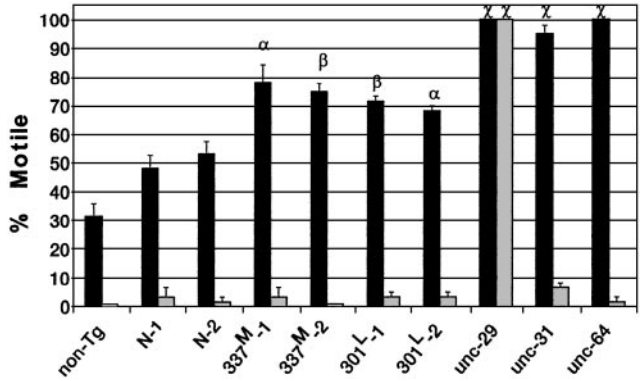

Fig. 2. Cholinergic neuronal transmission. Worms incubated in aldicarb (dark bars) or levamisole (light bars) were assessed for motility (36). Each bar is the average of three independent experiments with 20 animals each. Symbols are for comparisons to N-1 (α, $P = 0.01$; β, $P < 10^{-2}$; χ, $P < 10^{-3}$). Strain *unc-29* is deficient for AChR, *unc-31* is deficient for Ca^{2+}-dependent activator protein for secretion (CAPS), and *unc-64* is deficient for syntaxin.

lines is consistent with the fact that these mutations cause FTDP-17.

Impaired Cholinergic Transmission. Neuronal transmission was probed by using aldicarb, an acetylcholinesterase (AChE) inhibitor, or levamisole, a nicotinic acetylcholine receptor (AChR) agonist. Both drugs produce hyperactive cholinergic synapses, muscle hypercontraction, and paralysis (20). Worms lacking a functional AChR [*unc-29* (17); postsynaptic defect], or defective in presynaptic Ca^{2+}-dependent vesicle release [*unc-31* (21) and *unc-64* (22); presynaptic defects] are resistant to aldicarb, but only the AChR-defective line is also resistant to levamisole (Fig. 2). All tau lines were partially aldicarb resistant, with 337^{M} and 301^{L} lines being more resistant than N-1 or N-2. In contrast, all tau lines were sensitive to levamisole, indicating intact postsynaptic transmission. Thus, tau expression causes a presynaptic defect in cholinergic neurotransmission.

Accumulation of Insoluble Tau. Insoluble tau accumulates in brains from tauopathy subjects. The presence of insoluble tau in Tg lines was evaluated by sequentially extracting worms with buffers of increasing solubilizing strengths (10) (Fig. 3*A*). The RAB fraction is soluble tau, the RIPA fraction is detergent extractable insoluble tau, and the FA fraction is detergent-insoluble tau that can be extracted with 70% formic acid. All Tg lines produced approximately equivalent amounts of soluble tau (RAB supernatant). In mixed stage worms (5- to 7-day-old worms comprise the most mass), insoluble tau was seen in all lines, with 337^{M}-1 having the most followed by 301^{L}-1. Lines 337^{M}-1 and 301^{L}-1 had 2.5- and 1.7-fold, respectively, more FA-insoluble tau compared with N-1. In contrast, day-1 animals had no RIPA- or FA-insoluble tau. Note that at day 1, 337^{M}-1 and 301^{L}-1 were already Unc (Fig. 1*B*). The appearance of insoluble temporally paralleled the increasing severity of the behavioral deficit in 337^{M}-1 (Table 1).

Tau Phosphorylation. Aggregated tau from all tauopathies is hyperphosphorylated at specific serines and threonines (7). Alkaline phosphatase treatment of either soluble or insoluble tau from Tg lines, reduced the apparent size of tau from ≈64 kDa to ≈60 kDa, indicating the Tg tau is also phosphorylated (data not shown). To determine what sites were phosphorylated, a panel of phospho-dependent antibodies was used that detect sites hyperphosphorylated in tauopathies (Fig. 3*B*). Normal and mutant tau were phosphorylated at all sites examined, with

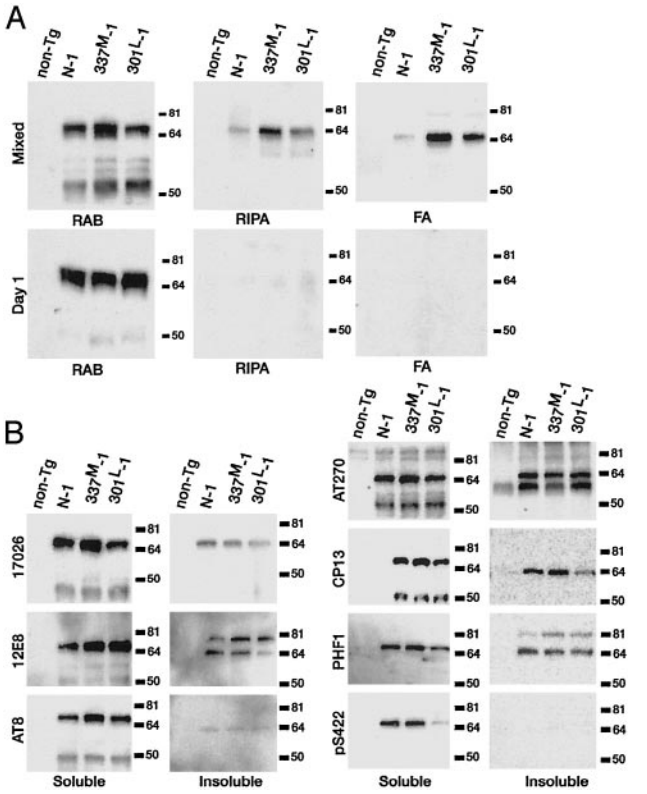

Fig. 3. (*A*) Tau solubility. RAB, RIPA, and FA fractions from equivalent amounts of packed mixed stage or 1-day-old worms were analyzed by immunoblotting using the phosphorylation-independent antibody 17026. (*B*) Tau phosphorylation. The soluble and insoluble proteins are the RAB supernatant and pellet, respectively. Fractions were analyzed by immunoblotting using antibodies that recognize the following tau phospho-epitopes: 12E8, S262; AT-8, S199, S202, and T205; AT-270, T181; CP13, S202; PHF-1, S396 and S404; pS422, S422.

limited qualitative differences observed between lines. Both soluble and insoluble tau were phosphorylated at most sites tested, except at serines 422 (antibody pS422), 199, and 202, and threonine 205 (antibody AT-8), where little or no phosphorylation was seen in the insoluble fractions. Thus, *C. elegans* neurons phosphorylate tau at many of the same sites phosphorylated in tauopathies. Tau from day 1 animals was also phosphorylated (not shown). In the soluble tau fraction, AT8, AT270, and CP13 detected an ≈50-kDa band that is presumably a tau proteolytic degradation product. PHF-1 and 12E8 reacted with an ≈80-kDa band in the insoluble fraction suggesting tau covalent crosslinking.

Tau Localization. Immunohistochemical staining of sectioned paraffin-embedded worms, and immunofluorescent staining of fixed whole animals showed tau localization consistent with

Table 1. Time course of insoluble tau accumulation

Time	Thrashes per min, mean ± SEM	RIPA tau, percent of total	FA tau, percent of total
Day 1	27.6 ± 3.3	0.8	0.09
Day 3	11.9 ± 2.3	9.8	4.2
Day 5	4.6 ± 1.4	5.0	10.6

Developmentally staged 337^{M}-1/glp-4 (bn2) animals were grown for 1, 3, and 5 days after hatching at 25°C. Thrashing rates are means from 10 animals. Tau in RAB, RIPA, and FA fractions were analyzed by quantitative immunoblotting using antibody 17026. Total tau is the sum of all fractions.

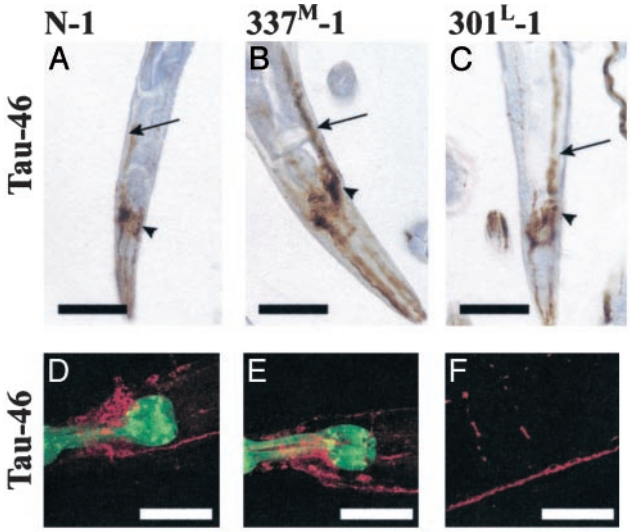

Fig. 4. Immunostaining for Tau. (*A–C*) Paraffin-embedded sections were stained with antibody Tau-46. (*D–F*) Whole mount animals were immunostained (37) by using Tau-46 as the primary antibody and AlexA 568 as the secondary antibody (red). GFP in the pharynx is green. Arrows point to the ventral nerve cord, and arrowheads are head neurons. No staining was seen in non-Tg animals (not shown). *D* and *E*, head; *F*, commissures, dorsal, and ventral nerve cords (see also Fig. 10, which is published as supporting information on the PNAS web site). (Scale bars = 50 μm.)

transgene expression in most if not all neurons (Fig. 4 and Fig. 8, which is published as supporting information on the PNAS web site). By both methods, Tau-46 reactivity was seen in the head as well as in dorsal and ventral nerve cords in both cell bodies and in neurites and in the interconnecting commissural axons. Immunostaining with Tau-2, CP13, AT8, and PHF-1 gave similar results (not shown).

Progressive Axonal Degeneration and Neuronal Loss. To visualize individual neurons, we crossed tau lines with *unc-25*::gfp (CZ1200), a line expressing GFP in 19 γ-aminobutyric acid (GABA)ergic inhibitory motor neurons (VD_{1-13} and DD_{1-6}) (23). In *unc-25*::gfp, both ventral and dorsal nerve cords are continuous and neuronal morphology is normal (Fig. 5*A*). In contrast, in double Tg lines (CZ1200/N-1, CZ1200/337^M-1, and CZ1200/301^L-1), there are axonal discontinuities, large inclusions, and exaggerated varicosities in both nerve cords (Fig. 5 *B* and *C*). Examination of an individual CZ1200/T337^M-1worm at ages 1, 5, and 7 days demonstrated the progressive nature of the degenerative changes (Fig. 5 *F–H*). At day 1 (Fig. 5*F*), all VD and DD motor neurons are present and the ventral and dorsal cords are essentially unaffected, though both cords appear faint in the posterior one-third of the worm. At day 5 (Fig. 5*G*), multiple dorsal and ventral cord discontinuities are evident, with the dorsal cord appearing more severely effected. Also, two inhibitory motor neurons are absent. By age 7 days (Fig. 5*H*), both dorsal and ventral nerve cords have with multiple gaps in each. Prominent cell body sized GFP-containing inclusions and/or exaggerated varicosities are seen in both cords.

Quantitation of dorsal and ventral cord gaps showed that the number of gaps increased slowly from day 1 to day 7 with little difference between line N-1 and the mutant lines. At day 9 there was a sharp increase in the number of gaps, with the FTDP-17 mutant lines showing significantly more gaps than N-1. All Tg lines showed progressive age-dependent neuronal loss with no difference between mutant and normal tau lines (Fig. 5*K*).

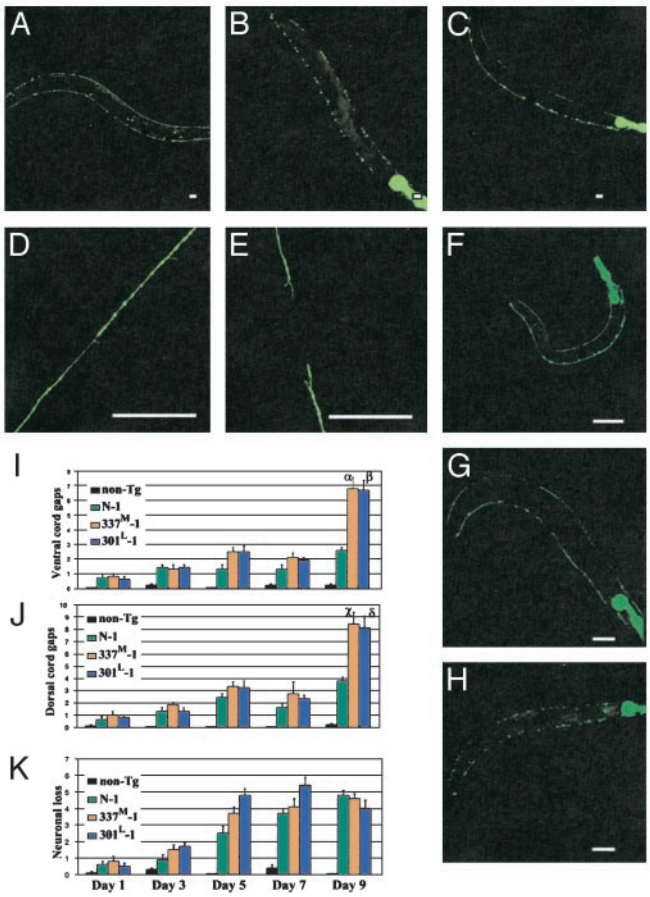

Fig. 5. Degeneration of γ-aminobutyric acid (GABA)ergic neurons. (*A–H*) GFP fluorescence in anesthetized living worms singly Tg for *unc-25*::GFP (*A*, 9 days old; *D*, mid-body dorsal nerve cord, 5 days old), doubly Tg for *unc-25*::GFP and 337^M-1 (*B*, 9 days old; *E*, mid-body dorsal cord, 5 days old), or doubly Tg for *unc-25*::GFP and 301^L-1 (*C*, 9 days old). Dorsal is up, and anterior is left. (Scale bar = 40 μm.) (*F–H*) GABAergic neuronal degeneration in a single 337^M-1/*unc-25*::GFP animal examined at age 1 day (*F*), 5 days (*G*), and 7 days (*H*). (*I–K*) Quantitation of dorsal cord (*I*) and ventral cord (*J*) gaps and neuronal loss (*K*) at different ages. Each measurement is the mean from 10 animals ± SEM. Symbols are for comparisons to N-1 (α, $P = 1 \times 10^{-3}$; β, $P = 2 \times 10^{-2}$; χ, $P = 3 \times 10^{-4}$; δ, $P = 3 \times 10^{-3}$).

Tau-Positive Aggregates in Degenerating Axons. Transmission EM and preembedding immuno-EM provided further evidence of neurodegeneration (Fig. 6 and Fig. 9, which is published as supporting information on the PNAS web site). Nine-day-old worms had no obvious abnormalities in neurons or axons in either the non-Tg (not shown) or N-1 animals (Fig. 6*A*). In contrast, irregularly oriented axons with vacuolar clearing of the axoplasm were frequent in 301^L-1 animals (Fig. 6*B*). More dramatic axonal degeneration was observed in 337^M-1 (Fig. 6 *C* and *D*); degenerating axons coursed irregularly in ventral and dorsal cord regions with extensive axonal dilations or axoplasmic clearing and collapse of axonal membranes and the intraaxonal compartment. These abnormal degenerating axons also contain spherical osmophilic aggregates (Fig. 6*D*). Immuno-EM revealed diffuse tau staining in the axons of N-1, 301^L-1, and 337^M-1 worms (Figs. 6 *E* and *F* and 9). Abnormal tau-positive aggregates in the degenerating axons were detected unequivocally only in 337^M lines (Fig. 6*F*). "Onion skin" membranous infoldings and whorls with associated amorphous tau accumulations were seen in 337^M-1 worms (Figs. 6*F* and 9), profiles characteristic of neurodegeneration in *C. elegans* (24). 337^M-1,

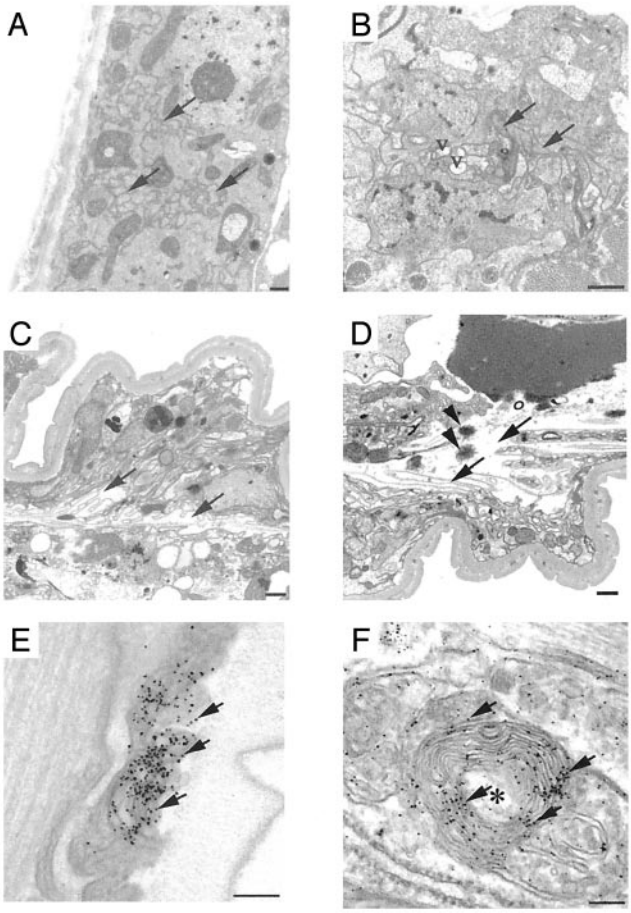

Fig. 6. Ultrastructural of degenerating axons. (*A–D*) Transmission EM. Transverse sections of 9-day-old N-1 (*A*), 301^{L}-1 (*B*), and 337^{M}-1 (*C* and *D*) lines. Arrows show normal axons in *A*, mildly degenerative axons in *B*, and severely degenerating disoriented axons in *C* and *D*. V, vacuolar clearing of axoplasm. Spherical, osmophilic protein aggregates (arrowheads) were evident (*D*). (*E* and *F*) Preembedding immuno-EM of 337^{M}-1 animals by using antibody 17026. The arrow shows immuno-silver-enhanced particles that identify tau-labeled structures. Degenerating axons with collapsed membranous profiles (onion skin lesions) are indicated by an asterisk and contain amorphous aggregates labeled by anti-tau antibodies. (Scale bars = 500 nm in *A–D* and 100 nm in *E* and *F*.)

which had the most extensive axonal degeneration, also had the highest levels of insoluble tau (Fig. 3*A*).

Discussion

The tau lines described here are a cellular and molecular model of FTDP-17 and other tauopathies. The first observed abnormality is uncoordinated movement that progressively worsens with age (Fig. 1*B*). This phenotype is followed by progressive accumulation of insoluble tau (Fig. 3*A* and Table 1), and neurodegeneration, observed as bulges and gaps in axonal tracks, followed by the loss of neurons (Fig. 5). By EM, neurodegeneration is observed as axonal vacuolar clearing, collapsed membrane structures and concentric layers of axonal membrane, a pattern characteristic of neuronal degeneration in *C. elegans* (Fig. 6). Axonal swelling, vacuolization, and axonal spheroids are also seen in *Drosophila* (25) and some mouse tau Tg models (10, 26, 27). Also, dilated axons were reported in an FTDP-17 multiple system atrophy family (3, 28). Both soluble and insoluble tau is phosphorylated at some of the same sites hyperphosphorylated in AD, FTDP-17, and other tauopathies (Fig. 3*B*).

FTDP-17 mutant lines had a more severe phenotype compared with normal tau lines, which is consistent with the role these mutations play in human disease. When compared with normal tau lines, 301^{L} and 337^{M} lines were more severely Unc, more resistant to aldicarb, accumulated more insoluble tau, and had more nerve cord gaps in old animals. Also, in axons, membrane whorls and loss of cytoplasmic density, features of severe degeneration, were only observed in the 337^{M} line (Fig. 6). FTDP-17 can also be caused by intronic (1) or silent *MAPT* mutations (29) that alter the isoform ratio but not the protein sequence of tau. Likewise, in *C. elegans*, normal tau lines did have a mild phenotype and were Unc by day 3 (Fig. 1*B*), accumulated aggregated tau (Fig. 3), and showed neuronal degeneration (Fig. 5).

C. elegans phosphorylates tau at some of the same sites hyperphosphorylated in AD and FTDP-17. However, tau phosphorylation did not appear to correlate with the severity of the phenotype. In day 1 adults, even though there was a difference between mutant and normal tau lines in behavior, there was no difference in the sites that are phosphorylated, nor any qualitative difference in immunostaining with phosphoepitope-dependent antibodies. However, these findings do not exclude the possibility that phosphorylation plays a role in the tau-induced phenotype. In tau transgenic *Drosophila*, phosphorylation increased with age and correlated with severity of neurodegeneration (25). Also, overexpression of *shaggy*, the fly homologue of glycogen synthase kinase-3β (GSK-3β) and a candidate kinase for tau phosphorylation, caused increased neurodegeneration, increased tau phosphorylation, and the appearance of filamentous tau aggregates (30). In contrast, in tau Tg mice, overexpression of GSK-3β alleviated transgene-induced motor neuron defects and axonopathy (31), even though GSK-3β overexpression increases tau phosphorylation (31–33). Thus, the role of phosphorylation in tau-induced neurotoxicity is unclear.

A distinct advantage of using *C. elegans* as a tauopathy model is that behavioral measures of neuronal dysfunction, neurodegeneration, and biochemical changes can be easily followed with time to establish the temporal sequence of pathogenesis. Impaired locomotion in the mutant lines (Fig. 1*B*) occurs before appreciable accumulation of insoluble tau (Fig. 3*A*), and before appreciable neuronal degeneration or loss. Thus, low-level tau aggregates such as dimers or small multimers may be sufficient to disrupt neuronal function. An alternative hypothesis is that aggregated tau is not essential for initial tau toxicity, and FTDP-17 mutations may produce a gain-of-function that affects other processes such as axonal MT transport (34). The results with aldicarb and levamisole (Fig. 2) demonstrate that Tg lines have a presynaptic defect. Transgene-induced abnormal axonal transport could cause abnormal presynaptic function. Insoluble tau did accumulate before gross neurodegeneration. Furthermore, mutant lines accumulated more insoluble tau and eventually showed more axonal loss (gaps) in the oldest animals. Therefore, although tau aggregation may not be required for the initial neuronal defect, it may contribute to the degenerative process that causes eventual neuronal loss.

In other tau Tg models, neurodegeneration is also observed without aggregated tau. In *Drosophilia*, Tg normal, $^{R}406^{W}$, or $^{V}337^{M}$ tau results in neuronal degeneration in the cortex, progressive appearance of disease-related tau phosphoepitopes, and reduced life span, but filamentous aggregated tau was not observed (25); aggregated tau appeared only when GSK-3β was also overexpressed (30). In mouse tau Tg models, the temporal sequence of events leading to overt neurodegeneration is less clear. In one model expressing $^{P}301^{L}$ tau, hindlimb weakness, as a measure of neuronal dysfunction, occurred coincidently with the appearance of aggregated tau and neurofibrillary tangles (27). In another model, aggregated and filamentous tau was

observed in the spinal cord at 6 months, whereas the number of Tg animals showing motor weakness did not begin to increase until 12 months of age (35). Although these later results imply that aggregated tau precedes neuronal dysfunction, hind limb function may not be an adequately sensitive measure of neuronal function. Thus, in mammals, because of the complexity of the nervous system and the lack of sensitive behavioral measures, it may be extremely difficult to establish cause and effect relationships for tau-induced pathogenesis.

The *C. elegans* model described here can be used to dissect the sequence of events leading to tau-induced neurodegeneration. Furthermore, genetic techniques can be applied to this worm model to identify genes that modify the tau-induced phenotype. Also, the tauopathy phenotype in these Tg worms is sufficiently robust for high-throughput screening for compounds that prevent tau-induced neuronal dysfunction and that are potential therapeutics for human tauopathies.

We thank Leo Anderson, Elaine Loomis, Lynn Greenup, Richard Green, Genn Merrihew, Barbara Pischek, Sarah Conyers, and Marlene Wright for excellent technical assistance. Antibodies PHF-1 and CP13 were from Peter Davies, 12E8 was from Peter Seubert (Elan Pharmaceuticals), and β-tubulin antibody E7 was from the Developmental Studies Hybridoma Bank (National Institute of Child Health and Human Development). Vector pPD49.26 was from Andy Fire. This work was supported by National Institutes of Health Grants AG17583 (to G.D.S. and J.Q.T.) and GM48700 (to J.H.T.), grants from the Virtual Research Institute, Nippon Boehringer Ingelheim Co., Ltd. (to G.D.S.), Alzheimer's Association Grant NIRG-02-3586 (to B.C.K.), and grants from the Department of Veterans Affairs.

1. Hutton, M., Lendon, C. L., Rizzu, P., Baker, M., Froelich, S., Houlden, H., Pickering-Brown, S., Chakraverty, S., Isaacs, A., Grover, A., *et al.* (1998) *Nature* **393,** 702–705.
2. Poorkaj, P., Bird, T. D., Wijsman, E., Nemens, E., Garruto, R. M., Anderson, L., Andreadis, A., Wiederholt, W. C., Raskind, M. & Schellenberg, C. D. (1998) *Ann. Neurol.* **43,** 815–825.
3. Spillantini, M. G., Murrell, J. R., Goedert, M., Farlow, M. R., Klug, A. & Ghetti, B. (1998) *Proc. Natl. Acad. Sci. USA* **95,** 7737–7741.
4. Hong, M., Zhukareva, V., Vogelsberg-Ragaglia, V., Wszolek, Z., Reed, L., Miller, B. I., Geschwind, D. H., Bird, T. D., McKeel, D. Goate, A., *et al.* (1998) *Science* **282,** 1914–1917.
5. Goedert, M., Jakes, R. & Crowther, R. A. (1999) *FEBS Lett.* **450,** 306–311.
6. Nacharaju, P., Lewis, J., Easson, C., Yen, S., Hackett, J., Hutton, M. & Yen, S. H. (1999) *FEBS Lett.* **447,** 195–199.
7. Buee, L., Bussiere, T., Buee-Scherrer, V., Delacourte, A. & Hof, P. R. (2000) *Brain Res. Rev.* **33,** 95–130.
8. K. Iwasaki, K., Staunton, J., Saifee, O., Nonet, M. & Thomas, J. H. (1997) *Neuron* **18,** 613–622.
9. Taub, J., Lau, J. F., Ma, C., Hahn, J. H., Hoque, R., Rothblatt, J. & Chalfie, M. (1999) *Nature* **399,** 162–166.
10. Ishihara, T., Hong, M., Zhang, B., Nakagawa, Y., Lee, M. K., Trojanowski, J. Q. & Lee, V. M. Y. (1999) *Neuron* **24,** 751–762.
11. Harlowe, E. & Lane, D. (1999) in *Using Antibodies: A Laboratory Manual* (Cold Spring Harbor Lab. Press, Plainview, NY), pp. 153–219 and 269–309.
12. Ishihara, T., Zhang, B., Higuchi, M., Yoshiyama, Y., Trojanowski, J. Q. & Lee, V. M. Y. (2001) *Am. J. Pathol.* **158,** 555–562.
13. Smith, C. M. & Swash, M. (1978) *Ann. Neurol.* **3,** 471–473.
14. Lee, V. M. Y., Balin, B. J., Otvos, L. & Trojanowski, J. Q. (1991) *Science* **251,** 675–678.
15. Barghorn, S., Zheng-Fischhofer, Q., Ackmann, M., Biernat, J., von Bergen, M., Mandelkow, E.-M. & Mandelkow, E. (2000) *Biochemistry* **39,** 11714–11721.
16. Gamblin, T. C., King, M. E., Kuret, J., Berry, R. W. & Binder, L. I. (2000) *Biochemistry* **39,** 14203–14210.
17. Lewis, J. A., Wu, C. H., Levine, J. H. & Berg, H. (1980) *Neuroscience* **5,** 967–989.
18. Thomas, J. H. (1990) *Genetics* **124,** 855–872.
19. McIntire, S. L., Garriga, G., White, J., Jacobson, D. & Horvitz, H. R. (1992) *Neuron* **8,** 307–322.
20. Nonet, M. L., Grundahl, K., Meyer, B. J. & Rand, J. B. (1993) *Cell* **73,** 1291–1305.
21. Avery, L., Bargmann, C. I. & Horvitz, H. R. (1993) *Genetics* **134,** 455–464.
22. Nguyen, M., Alfonso, A., Johnson, C. D. & Rand, J. B. (1995) *Genetics* **140,** 527–535.
23. Jin, Y., Jorgensen, E., Hartwieg, E. & Horvitz, H. R. (1999) *J. Neurosci.* **19,** 539–548.
24. Hall, D. H., Gu, G., Garcia-Anoveros, J., Gong, L., Chalfie, M. & Driscoll, M. (1997) *J. Neurosci.* **17,** 1033–1045.
25. Wittmann, C. W., Wszolek, M. F., Shulman, J. M., Salvaterra, P. M., Lewis, J., Hutton, M. & Feany, M. B. (2001) *Science* **293,** 711–714.
26. Spittaels, K., Van den Haute, C., Van Dorpe, J., Bruynseels, K., Vandezande, K., Laenen, I., Geerts, H., Mercken, M., Sciot, R., Van Lommel, A., *et al.* (1999) *Am. J. Pathol.* **155,** 2153–2165.
27. Lewis, J., McGowan, E., Rockwood, J., Melrose, H., Nacharaju, P., Van Slegtenhorst, M., Gwinn-Hardy, K., Murphy, M. P., Baker, M., *et al.* (2000) *Nat. Genet.* **25,** 402–405.
28. Spillantini, M. G., Goedert, M., Crowther, R. A., Murrell, J. R., Farlow, M. R. & Ghetti, B. (1997) *Proc. Natl. Acad. Sci. USA* **94,** 4113–4118.
29. D'Souza, I., Poorkaj, P., Hong, M., Nochlin, D., Lee, V. M. Y., Bird, T. D. & Schellenberg, G. D. (1999) *Proc. Natl. Acad. Sci. USA* **96,** 5598–5603.
30. Jackson, G. R., Wiedau-Pazos, M., Sang, T. K., Wagle, N., Brown, C. A., Massachi, S. & Geschwind, D. H. (2002) *Neuron* **34,** 509–519.
31. Spittaels, K., Van den Haute, C., Van Dorpe, J., Geerts, H., Mercken, M., Bruynseels, K., Lasrado, R., Vandezande, K., Laenen, I., Boon, T., *et al.* (2000) *J. Biol. Chem.* **275,** 41340–41349.
32. Brownlees, J., Irving, N. G., Brion, J. P., Gibb, B. J. M., Wagner, U., Woodgett, J. & Miller, C. C. J. (1997) *NeuroReport* **8,** 3251–3255.
33. Lucas, J. L., Hernandez, F., Gomezramos, P., Moran, M. A., Hen, R. & Avila, J. (2001) *EMBO J.* **20,** 27–39.
34. Stamer, K., Vogel, R., Thies, E., Mandelkow, E. & Mandelkow, E. M. (2002) *J. Cell Biol.* **156,** 1051–1063.
35. Higuchi, M., Ishihara, T., Zhang, B., Hong, M., Andreadis, A., Trojanowski, J. Q. & Lee, V. M. Y. (2002) *Neuron* **35,** 433–446.
36. Daniels, S. A., Ailion, M., Thomas, J. H. & Sengupta, P. (2000) *Genetics* **156,** 123–141.
37. Crittenden, S. L. & Kimble, J. (1999) *Methods Mol. Biol.* **122,** 141–151.